Article

Combining Microstructured Surface and Mesh Covering for Heat Transfer Enhancement in Falling Films of Refrigerant Mixture

Oleg Volodin *, Nikolay Pecherkin and Aleksandr Pavlenko *

Kutateladze Institute of Thermophysics, Siberian Branch of the Russian Academy of Sciences, 1 Lavrentyev Ave., 630090 Novosibirsk, Russia
* Correspondence: volodin@ngs.ru (O.V.); pavl@itp.nsc.ru (A.P.)

Abstract: The article presents the experimental results of combining a basic microstructure with partly closed pores and a mesh covering for heat transfer enhancement at the film flow of a refrigerant mixture. To reveal the effect of the combined structure, heat transfer on a microstructured surface without a covering as well as on a smooth surface with a mesh covering only has been studied. All experimental series were carried out using a binary mixture of R114 and R21 refrigerants. The mixture film flowed down the outer surface of a vertical cylinder in the undeveloped turbulence regime, when the film Reynolds number varied from 400 to 1300. It is shown that a microstructured surface with a fin pitch of 200 μm, fin height of 220 μm, and longitudinal knurling pitch of 160 μm, created by deformational cutting, demonstrates significant heat transfer enhancement: up to four times as compared to a smooth surface. However, adding a mesh covering with an aperture of 220 μm and a wire diameter of 100 μm reduces the intensification. The mesh covering overlaid on a smooth surface also does not provide heat transfer enhancement as compared to the smooth surface itself. The absence or even deterioration of heat transfer enhancement on surfaces with mesh covering can be primarily associated with the low thermal conductivity of the mesh material and shortcomings of the applied method of mesh mounting. The possibility of deteriorating vapor removal due to the incorrect selection of mesh covering parameters was also analyzed. The heat transfer coefficient values obtained for basic microstructured surfaces were compared with the dependencies available in the literature for predicting pool boiling heat transfer on microfinned surfaces.

Keywords: nucleate boiling; combined coating; deformational cutting; mesh covering; falling films; refrigerant mixture

1. Introduction

The study of heat transfer in falling films of liquids and their mixtures is important for improving the efficiency of numerous systems using film flows—from natural gas liquefaction (LNG) plants, distillation plants, and absorption apparatuses, as well as evaporative equipment of the chemical and food industries—to desalination plants and electronic equipment cooling systems (e.g., spray and falling-film cooling system [1]). The intensification of heat transfer at boiling and evaporation of liquids by structuring the heat-generating surface is a key method for increasing the efficiency of both traditional [2–5] and renewable [6] energy systems. Despite the fact that studies on heat transfer enhancement have been actively carried out since the middle of the last century, their relevance at the current pace of technology development is only increasing. Among various types of structured coatings (including capillary-porous), wire mesh coverings—which can be attributed to the simplest porous coatings—are among the most accessible and easily modified. The advantages of these coverings also include: ease of installation, high scalability, low production cost, and reproducibility of the geometric parameters of wire meshes. All this determines the renewed interest in recent years in the use of mesh coverings in various configurations [5].

For a rather long period of research on the use of mesh coverings of heating surfaces for heat transfer enhancement, i.e., from about 1975 and until the end of the first decade of the 21st century, not so many promising results were obtained on increasing the heat transfer coefficient (HTC) or delaying of reaching the critical heat flux (CHF) [5]. It was generally believed that mesh coverings enhance heat transfer at low heat fluxes and impair it at high heat fluxes. The enhancement was associated with the increased area of the mesh-covered surface and consequently the higher number of active nucleation sites, whereas at higher heat fluxes heat transfer becomes dependent on the vapor removal, and in this case, the mesh coatings (especially multilayer ones) impair heat transfer [5,7].

However, the results of studies conducted over the past decade [5] show that mesh coverings can be an effective means of heat transfer enhancement in a wide range of heat flux changes. Some authors have also expanded previous ideas [7] about the causes of the HTC improvement by introducing fresh concepts like "micro-chimney effects" and "gradient mesh coatings" [6]. The desired enhancement can be realized provided that the mesh geometrical parameters, the number of mesh layers, the wire material, and the mesh mounting method are optimally chosen. Thus, significant heat transfer enhancement was obtained using the mentioned above gradient mesh coatings [6] (HTC enhancement up to 6.6 times), as well as uniform layers mesh coatings at atmospheric (HTC enhancement from about 3 [8] to 10 times [9]) and subatmospheric pressures (HTC enhancement up to 22 times [9]). Promising results have also been achieved by combining mesh covering with other types of surface treatment: microfinning, nanostructuring, mesh with cells filled with powder from micro-nanoparticles, as well as when processing wire mesh itself.

Below we briefly review the works devoted to the study of heat transfer enhancement and the increase of the critical heat flux using multilayer or combined mesh coatings, which contain the most interesting or promising results in the opinion of the authors.

In the works [10,11], it was demonstrated that covering a rough surface with a mesh can reduce the intensity of heat transfer. Trying to use simple and practical methods of enhancement, Tsay et al. [10] were among the first to combine the roughening of heat transfer surface with a mesh covering (from stainless steel AISI 304) to enhance boiling in thin layers of water on a horizontal plate (also from AISI 304) of 10 cm length, 2.5 cm width, and 0.1 cm thickness. The authors also investigated the effect of applying various mesh coverings (mesh 16, 24, and 50) to a smooth plate. As a result, it received up to a sevenfold HTC increase (at liquid level H = 5 mm and mesh 16) at low heat fluxes. The thinner the liquid layer, the greater the observed enhancement. However, no additional enhancement for the mesh-covered rough surfaces as compared with the mesh-covered smooth ones was received.

The use of combined coatings by Brautsch and Kew [11] was also unsuccessful in terms of heat transfer enhancement. The authors used low carbon stainless steel AISI 304L meshes (mesh 50, 100, 150, and 200), as well as two heat-releasing surfaces with R_a = 0.42 μm and R_a = 1.04 μm, to study heat transfer enhancement in the saturated pool boiling of water on the vertical test section. They showed that both techniques—roughening of surface and covering the heater with a mesh, are effective. However, combining them was shown to be ineffective, resulting in the HTC deterioration even as compared to the smooth surface.

Despite these and other unsuccessful experiments on heat transfer enhancement [5], changes in the material and method of mounting mesh coverings allowed Sloan et al. [9] to achieve significant intensification of HTC over the entire range of heat fluxes. The authors [9] studied the pool boiling of water at subatmospheric pressure on a 4 cm^2 vertically oriented copper circular disk, covered with 1–8 layers of copper mesh. It was shown that eight-layer mesh 145 covering demonstrated about a 10-fold HTC increase (at ΔT = 10 K) at atmospheric pressure and a 22-fold increase (at ΔT = 8 K) at subatmospheric pressure (0.2 atm). It is worth noting that Sloan et al. used copper mesh coverings previously cold-rolled to increase the available surface area for the diffusion bonding process by producing flat spots on the high points of each wire.

Chien and Tsai [12] studied heat transfer at film flow and pool boiling of R-245fa at different saturation temperatures on horizontal finned copper tubes (of 0.4 mm fin height, 60 FPI) and the same tubes, covered with copper mesh. They achieved a notable HTC enhancement—up to four and seven times at pool boiling of R-245fa for 5 and 20 °C, respectively, and up to five times at film flow of R-245fa, compared to a smooth tube. For comparison, the uncovered finned tube in the latter case provided intensification only 3.5 times.

The authors [13] used a combined surface with brass or copper meshes (mesh 80, 100, and 120) covered finned horizontal tubes with fins of 0.2–0.4 mm high. Pool boiling of R-134a at saturation temperatures of 5, 10, and 26.7 °C was enhanced 2–3 times. The best performance was achieved by wrapping a brass mesh 100 on a tube with 0.4 mm fin height—up to 8 times (peak value) compared to an uncovered tube.

Kim et al. [14] achieved 84% CHF enhancement by using single-layered stainless steel mesh (with wire diameter $0.29 \div 0.7$ mm and mesh aperture $1.29 \div 2.67$ mm range) with micro/nano-sized pore structure of meshes applied to SiO_2 heating surface at water pool boiling. The authors underlined that their method of increasing CHF does not require any modifications of the heating surface and can be easily adopted in different technical applications (for example, to create IC chip coatings).

Dąbek et al. [15] studied the pool boiling of water and ethyl alcohol on a horizontal copper heater of 30 mm diameter with copper or bronze one- or two-layer mesh coatings at atmospheric pressure. The possibility of sevenfold and fourfold enhancement as compared to a smooth surface (at superheat of about 8 K) for copper meshes with apertures of 0.75 mm and 0.2 mm, respectively, has been demonstrated.

The work of [16] is notable for the fact that the authors used 3D-printed mesh structures for heat transfer enhancement at the pool boiling of water at the saturation line. A total of 12 samples were divided into two groups of printed meshes: "thin" (0.75 mm wall height) and "thick" (1.5 mm wall height), with pitch varied in a range of $0.4 \div 1.3$ mm. Stainless steel 316 L powder was used in the process of selective laser melting (SLM). Zhang et al. [16] showed the possibility of a threefold CHF enhancement as compared to a smooth surface by applying a mesh with 1.1 mm pitch ("thick"), also HTC enhancement of two to three times by applying meshes with 0.5 mm pitch ("thin") and 0.7–1.1 mm pitch ("thick") as compared to the smooth surface was achieved. This work [16] demonstrates the perspectives of additive manufacturing (AM) for creating prototypes of samples with precisely controlled structure parameters.

Pastuszko et al. [17] used micro-finned surfaces with copper mesh covering as well as micro-finned surfaces covered by copper perforated foil at pool boiling of water, ethanol, Novec-649, and FC-72 at atmospheric pressure. Microfins covered with wire mesh produced the highest HTC among studied surfaces at medium and high heat fluxes for water, low and medium heat fluxes for ethanol, and medium heat fluxes for FC-72.

The authors of [6] have demonstrated that multilayer mesh coatings can be highly efficient intensifiers by studying the pool boiling of distilled water at the saturation line on a heated surface covered with multi-layer mesh. Four configurations of six-layer copper mesh coverings with gradient (direct or inverse) or uniform porosity were studied. It was shown that a six-layer mesh (3 + 3) with coarser three upper layers gives a maximum HTC enhancement—up to 6.6 times (261 kW/m²K), along with a three-fold enhancement in CHF (outstanding 2719 kW/m²). The authors associate the obtained enhancement results with so-called "micro-chimney effects" [6], taking place in gradient porous micro meshes.

Huang et al. [18] applied four hybrid surfaces for heat transfer enhancement at sub-cooled water flow boiling in channels (at a pressure of 0.5 MPa, a flow velocity of 1–5 m/s, and an inlet temperature of 298 K). The authors used wire mesh coatings combined with a powder mixture of micro/nanoparticles of Ag, Cu, and Ti. Heat flux removed by combined surfaces was two to three times higher than heat flux removed by the smooth surface, CHF for the investigated surfaces increased by 80–200%.

The authors [19], as well as [6] demonstrate the effectiveness of multilayer gradient meshes, but in terms of enhancement of wicking capability. It was shown that the wicking capability of a multilayer gradient mesh consisting of three lower layers of a mesh 100 and three upper layers of a mesh 300 is significantly enhanced compared to wicks consisting of a multilayer mesh with identical layer characteristics.

In the previously mentioned work [8] the authors proposed a surface, sintered with multilayer copper meshes having identical geometrical characteristics (mesh 200 with 30 µm wire diameter), studying the water pool boiling. It is shown that an increase in the number of layers (up to 5) can reduce the size of the micropores, increasing the density of nucleation sites and improving capillary wicking performance, thus improving the HTC and delaying the boiling crisis development. The multilayer mesh with 5 layers demonstrates optimal boiling performance, providing the highest CHF of 208 W/cm^2 and the highest HTC of 16 W/(cm^{2}K). The authors made the conclusion that the remarkable boiling performance along with the low cost, simplicity, and high durability of mesh coatings show the industrial prospects for commercial compact microelectronics cooling.

Hu et al. [20] along with the authors of [8,9] demonstrate the perspectives of using uniform multilayer copper micromeshes for heat transfer enhancement, in particular, to increase heat transfer proportion of liquid film boiling in spray cooling of 10×10 mm^2 target surface. It is shown that a four-layer mesh 100 covering (mesh covering with 50 µm wire diameter and 204 µm aperture) fabricated by diffusion bonding, exhibits the best heat transfer performance with CHF of 605 W/cm^2 and maximum HTC of 71 kW/(m^{2}K), which corresponds to enhancing by 127% and 176%, compared with the uncovered surface, respectively.

Thus, the above shows that wire mesh coatings in various combinations and modifications can be an effective means of boiling heat transfer for a wide spectrum of technical applications, including apparatuses using pool boiling [6–9,11–17], working at low pressures [9], using spray cooling [20], thin layers of liquid [10], film flow [7,12], or microchannels [18]. The aim of this work is to initiate the investigation of the efficiency of combined coatings for heat transfer enhancement in the binary refrigerant mixture films falling down the outer surface of a vertical cylinder. Despite the fact that the cooling of heating surfaces by falling films does not allow the removal of large heat fluxes as in the case of the recognized leader among cooling methods—spray irrigation, which makes it possible to remove heat fluxes up to 1000 W/cm^2 [21], tubular heat exchangers operating at low and moderate heat fluxes are widely used and in demand in the industry (for example, in LNG systems), and the possibility of enhancing heat transfer and improving the ergonomics of film evaporators by using tubes with modified surfaces requires systematic research in this field.

2. Experimental Setup and Procedure

2.1. Test Sections

To create the basic microstructure with halfway-closed micropores, providing more effective nucleate boiling, the previously well-established method of deformational cutting (MDC) was used [22–24]. The microstructure, created on the outer surface of a copper cylinder with a diameter of 50 mm and wall thickness of 1.5 mm, has the next geometrical parameters: fin pitch—200 µm, fin height—220 µm, and longitudinal knurling pitch—160 µm (Figure 1a,b). The knurling over microfinning, crushing the tops of the fins with a decrease in its height by 35%, is carried out in order to create the halfway-closed pores surface. In the work of [22], it was shown the effectiveness of such structure type for nucleate boiling enhancement. In this study, we slightly modified the parameters of the most effective MDC-surface (microstructure No. 1 from [22]), increasing its fin pitch (from 100 µm to 200 µm)—with the aim of improving vapor removal, and reducing its knurling pitch (from 318 µm to about 160 µm)—in attempt to increase the amount of nucleation centers.
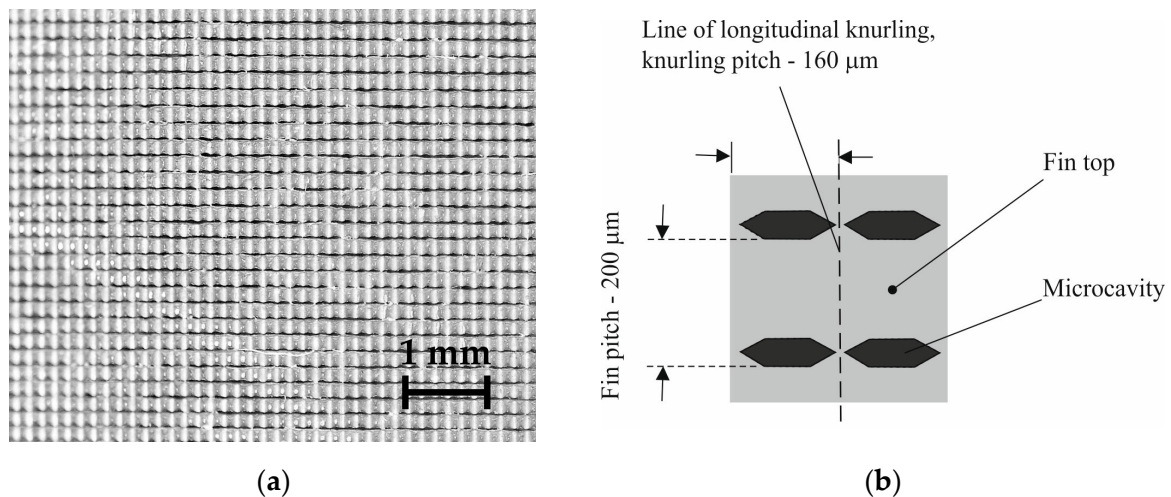
Figure 1. (**a**) photograph of the surface, structured by deformational cutting, (**b**) sketch of the element of the MDC-surface.

At the next stage of test section preparation, the stainless steel mesh (AISI 304) with an aperture of 220 μm and wire diameter of 100 μm was tightly wrapped around the microstructured tube, fixed, and then soldered with a slight overlap of layer upon layer. Resulting in a combined structure (Figure 2a), the single element of which is shown (according to scale) in Figure 2b. The characteristics of mesh were chosen so as to approximately correspond to the parameters of the basic structured surface since a finer upper mesh would impair vapor removal, while a too-coarse upper mesh would not have an effect on the nucleate boiling process.
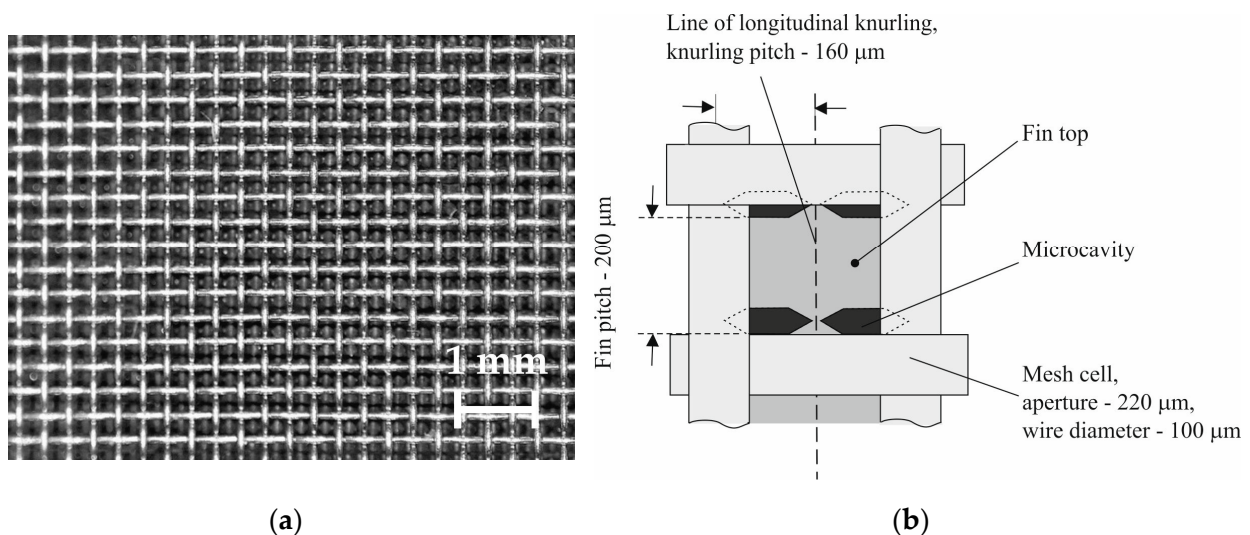
Figure 2. (**a**) photograph of the combined surface, (**b**) sketch of the element of the combined surface.

In addition to applied steel mesh coverings (which did well in [10] and some other works, despite the low thermal conductivity of steel), in the next stage of the study, it is planned to use copper and brass meshes; the geometric parameters of meshes and applied installation methods will also vary.

To reveal the effect of the combined coating structure on heat transfer intensification, the heat transfer on the microstructured surface without mesh covering as well as on a smooth surface with mesh covering alone and on an uncovered smooth surface were also studied. All types of test sections used in the study are listed in Table 1.

Table 1. Types of test sections used in the study.

Test Section Type	Material	Geometrical Parameters
Smooth tube	Copper M1	smooth tube with roughness R_a = 2.5 μm
Microstructured tube	Copper M1	microstructure with fin pitch 200 μm, fin height 220 μm and knurling pitch 160 μm
Smooth tube + mesh	Copper M1 + AISI 304	smooth tube with R_a = 2.5 μm + mesh with aperture 220 μm and wire diameter 100 μm
Microstructured tube + mesh	Copper M1 + AISI 304	microstructure with fin pitch 200 μm, fin height 220 μm and knurling pitch 160 μm + mesh with aperture 220 μm and wire diameter 100 μm

*2.2. Experimental Setup and Parameters*

The experiments were carried out in the test column (1) 1.5 m high and with an inner diameter of 0.27 m under saturation conditions at an absolute pressure of about 2 bar (Figure 3a,b). A more complete arrangement of the experimental setup is given in [25]. The R114/R21 refrigerant mixture is fed into a constant-level tank (2) from where it comes through the slot distributor to the test section (3). The local temperatures of the heating wall are controlled by five copper-constantan thermocouples (4) with a wire diameter of 0.15 mm, embedded flush with the wall surface and located vertically along the heated area having a length of 70 mm with a step of 13 mm. Thermocouples are handcrafted and calibrated over a range of operating temperatures (20–55 °C) using the proven reference thermometer (LT-300). The diameter of the thermocouple bead does not exceed 0.7 mm. The sensitivity of copper-constantan (CuKn) thermocouples or type T thermocouples is about 40 microvolts per degree. The use of a highly sensitive voltmeter APPA 207 made it possible to measure thermo-EMF values with an accuracy of ±8 μV. The cold junctions of thermocouples (5) are located at the bottom of the column, immersed in the liquid layer. The temperatures in the different sections of the column are controlled by platinum thermoresistors HEL-711-U-0-12-00 (6) by Honeywell. The HEL-711 temperature sensors allow the measurement of temperature in the range of −200 to +260 °C with an accuracy of ±0.1%. One of the thermistors located at the bottom of the column together with cold junctions of thermocouples in order to measure the temperature of the liquid to correctly build the dependence of the wall temperature on the thermo-EMF, taking into account the temperature fluctuations of the liquid at the column bottom.

The observations and high-speed shooting (by Phantom VEO 410 L) of processes, developing in the heated area, are carried out through three quartz optical windows (7). The pressure in the test volume is measured using a manometer Metran-100 (8).

Stabilized supply source Mastech HY10010E was used to heat the test section, capable of providing heat fluxes up to critical. The load was raised stepwise, the readings were taken while moving up the heat flux branch after the heater temperature reached a stationary value (which took about 10–15 min, depending on the heat transfer regime). The binary mixture film flowed down the vertical cylinder in the undeveloped turbulence regime with the film Reynolds number at the inlet of the test section varied from 400 to 1300. The film Reynolds number was determined as:

$$Re = \frac{4G}{\pi d \mu}, \tag{1}$$

here *G* is mass rate, *d*—tube diameter, and *μ*—dynamic viscosity. The mass flow rate was measured by the Coriolis flow meter CORI-FLOW M55.
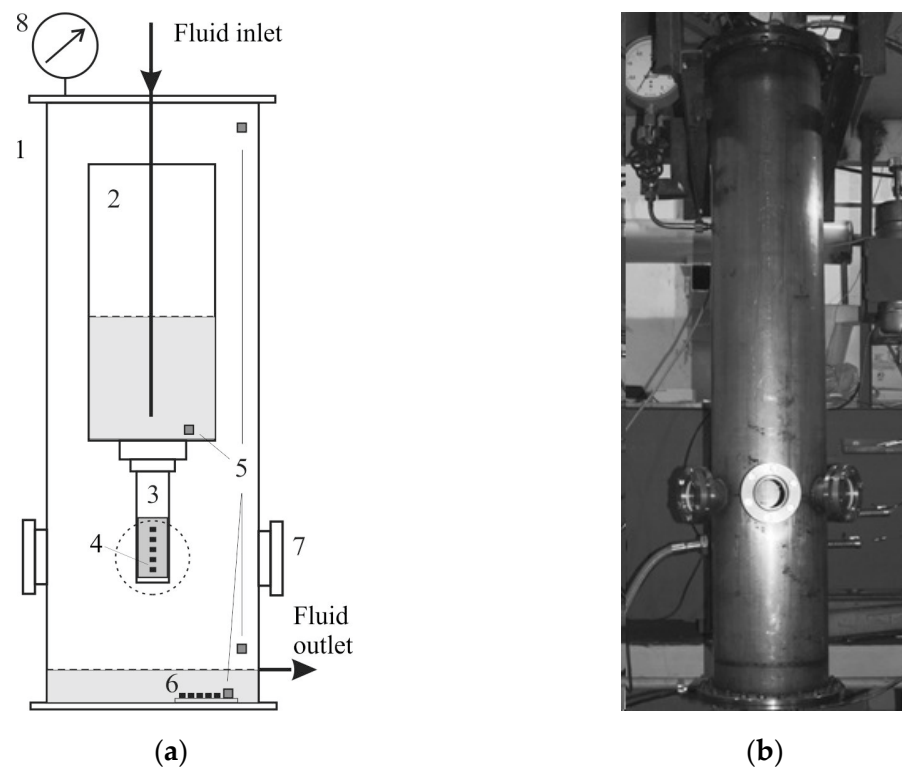
Figure 3. The scheme of the test column (**a**): 1—sealed column; 2—constant level tank; 3—test section; 4—heated zone of the test section with thermocouples; 5—thermal resistors; 6—thermocouples cold junctions; 7—optical windows; 8—a manometer. The photograph of the test column without heat shield (**b**).

The distance from the slot distributor to the beginning of the heated area was equal to 100 mm, which noticeably exceeded the distance of hydrodynamic stabilization of the flow in all studied ranges of the flow rates; a corresponding estimation was carried out in [22].

The selected R114/R21 refrigerant mixture has low surface tension, high wettability, and low viscosity, which makes it convenient for modeling heat transfer processes for a wide class of low-viscosity technical fluids. In addition, the presence of the volatile component of the mixture (R114) can notably enhance the heat transfer process. In the work of [26], it was shown that for a 10% mixture of R114/R21, the heat flux density corresponding to the onset of boiling (ONB) was reduced by half as compared to pure R21, and an increase in HTC up to 2.5 times was observed in the range of heat fluxes q: $0.1 \div 10$ W/cm^2. It can also be noted that the use of a non-azeotropic mixture can increase the critical heat flux value, due to the later evaporation of the low-boiling component [27,28]. With this in mind, a mixture of R114 and R21 refrigerants with an initial concentration of volatile component R114 of about 12% (the mixture behaves as non-azeotropic at this concentration) was chosen as the working fluid.

2.3. Experimental Procedure and Data Reduction

Before the start of each experimental series (and after the tightness test), vacuum evacuation of the test volume was performed to degas the volume and the micropores of the test section. To evacuate the test setup (remove air) before filling it with the working fluid, an RV-40 forevacuum pump was used. Air was pumped out to a residual pressure of 6–8 Pa. After air was evacuated from the test setup, the setup volume was filled with vapors of the working fluid from the storage vessel. At room temperature of about (20–22) °C, the excess pressure in the setup is maintained at the level of (0.5–0.6) bar, which excludes air suction into the setup. Measurement of vapor pressure and vapor and liquid phase

temperatures in the test volume made it possible to control the state of saturation of the working fluid and the absence of impurities (like air) during the experiments.

To measure the local wall temperatures, the thermo-EMF values from five thermocouples were recalculated into temperature values using a two-dimensional regression—the function of thermo-EMF and the temperature of cold junctions.

The heat flux density was calculated by the formula:

$$q = C \frac{I^2 R}{A}, \tag{2}$$

here, *C* is a correction factor taking into account heat losses due to the heat conductivity of the test section. According to the numerical calculations performed for the studied test sections, the heat loss due to longitudinal heat conductivity of cylinder walls did not exceed 5%. The areas of the modified heat-releasing surfaces *A* during calculations were taken equal to the area of the covered smooth surface.

The local heat transfer coefficients were determined by the standard formula:

$$h = \frac{q}{(T_w - T_s)}, \tag{3}$$

here T_W—temperature of the wall, T_S—saturation temperature.

The uncertainty in determining the local heat transfer coefficient *h* consisted of uncertainties in determining the heat flux *q* and the wall superheat temperature $\Delta T = (T_w - T_s)$.

The final uncertainty of the heat transfer coefficient $h = f(q, \Delta T)$ was calculated by the formula:

$$U^2(h) = \sum_{i=1}^{N} \left(\frac{\partial f}{\partial x_i} \right)^2 U^2(x_i) \tag{4}$$

or

$$\left(\frac{U(h)}{h} \right)^2 = \left(\frac{U(q)}{q} \right)^2 + \left(\frac{U(\Delta T)}{\Delta T} \right)^2, \tag{5}$$

where $U^2(\Delta T) = U^2(T_w) + U^2(T_s)$.

According to the assessment, the maximum error when determining ΔT was introduced by the relative uncertainty of T_w, measured by CuKn thermocouples, that did not exceed 10% at $\Delta T > 2\,°C$. So the uncertainty of $\Delta T = (T_w - T_s)$ will also not exceed 10% up to the integer. The relative uncertainty of the heat flux *q* taking into account heat losses did not exceed 6%. Thus the relative uncertainty of the local heat transfer coefficient *h* did not exceed 12% at $\Delta T > 2\,°C$.

3. Results and Analysis

Figure 4a–d illustrates the boiling process of the R114/R21 mixture falling film on studied test sections at the initial stages of nucleate boiling. The test sections structured by deformational cutting, both uncovered (Figure 4b) and having mesh covering (Figure 4d), demonstrate a more effective nucleation process than sections without basic MDC-structuring (Figure 4a,c), with nucleation sites activated from the beginning of heating area—so it becomes visible—to its end.

Figure 5a–d demonstrate the nucleate boiling of binary mixture falling film on studied sections at developed boiling regime—with the presence of very large bubbles (see for example Figure 5c) characteristic of the mixtures and according to our observations does not occur in pure refrigerants. Again it can be noted that both test sections with substrate structured by deformational cutting (Figure 5b,d) demonstrate a more effective nucleation process with nucleation sites evenly distributed over the entire heat-releasing surface. Next will be shown that the heat transfer data confirm the visual observation.
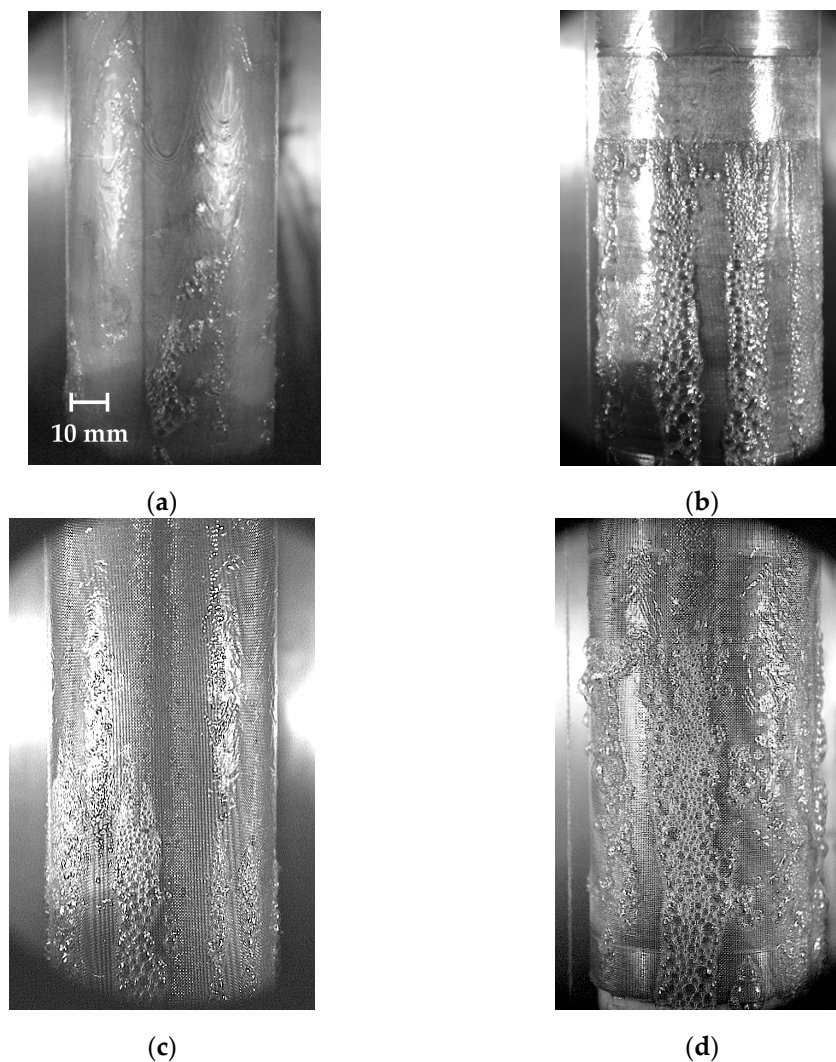
Figure 4. Inception of nucleate boiling of R114/R21 mixture on: (**a**) smooth ($q = 1.7 \, \text{W/cm}^2$, *Re* = 640), (**b**) microstructured by MDC ($q = 1.7 \, \text{W/cm}^2$, *Re* = 640), (**c**) smooth covered by mesh ($q = 1.7 \, \text{W/cm}^2$, *Re* = 845) and (**d**) combined ($q = 1.7 \, \text{W/cm}^2$, *Re* = 640) surfaces.

Boiling curves obtained for the investigated surfaces are shown in Figure 6a–d.

Figure 6a shows the boiling curve for the smooth surface. In the film evaporation regime ($q \leq 1 \, \text{W/cm}^2$), the flow rate does not affect heat transfer. For all Reynolds numbers, ONB takes place at $q \geq 1 \, \text{W/cm}^2$ and incipience superheat $\Delta T \approx 8$ K, respectively. Above $\Delta T \approx 8$ K and up to the developed boiling regime ($\Delta T \approx 10.5$ K), an insignificant effect of the flow rate on heat transfer is observed—the thinner the film, the higher heat transfer, as a rule. This could be due to the different contributions of evaporation to heat transfer, which takes place for different thicknesses of the falling film in the developing boiling regime. However, this effect is weakly expressed, and the presence of any kind of microtexture (Figure 6b–d) immediately shuffles the cards.

Microstructured surface by the method of DC (Figure 6b) demonstrates the greatest heat transfer efficiency, while the presence of the mesh covering does not affect (Figure 6c), or even worsens (Figure 6d), the heat transfer process. In the first case, we suppose, this is due to the fact that stainless steel (AISI 304) mesh used in the experimental series has a low thermal conductivity (15 W/mK), and the method of mesh attachment used is apparently not effective enough to create an ideal mesh-heated surface contact. In the case of combined surface, this also can be connected with the fact that we did not choose the

mesh covering parameters well enough for our experimental conditions, which may cause the deterioration of vapor removal.

Thus, despite the fact that the presence of an applied steel mesh covering to some extent orders nucleate boiling (one can compare boiling patterns on mesh-covered surfaces in Figure 4c,d and on the smooth one in Figure 4a), taking into account the deterioration of heat transfer, at the next stage of the experiment, measures should take into account the existing shortcomings of the mesh coating used. It is planned to use highly thermally conductive copper mesh coatings and the process of sintering to ensure contact of the mesh covering with the heated surface; a more careful selection of mesh covering parameters also should be provided.

A comparison of experimental data on HTC and its enhancement on the studied surfaces for the range of Reynolds number $400 \div 1300$ is presented in Figure 7a,b. As noted above, the presence of mesh with the given characteristics does not enhance the boiling process when covering the smooth surface: data on HTC coincide with data for a smooth surface, Figure 7a. The microstructured surface, created by deformational cutting (Figure 7b), demonstrates the greatest heat transfer enhancement (up to four times as compared with the smooth one). In the case of mesh overlay of the microstructured surface (i.e. in the case of combined coating), even impairment (up to two times) in heat transfer as compared to high-performance MDC-surface is observed, Figure 7b.

(a)　　　　　　　　　　　　　　　　　　　　(b)

(c)　　　　　　　　　　　　　　　　　　　　(d)
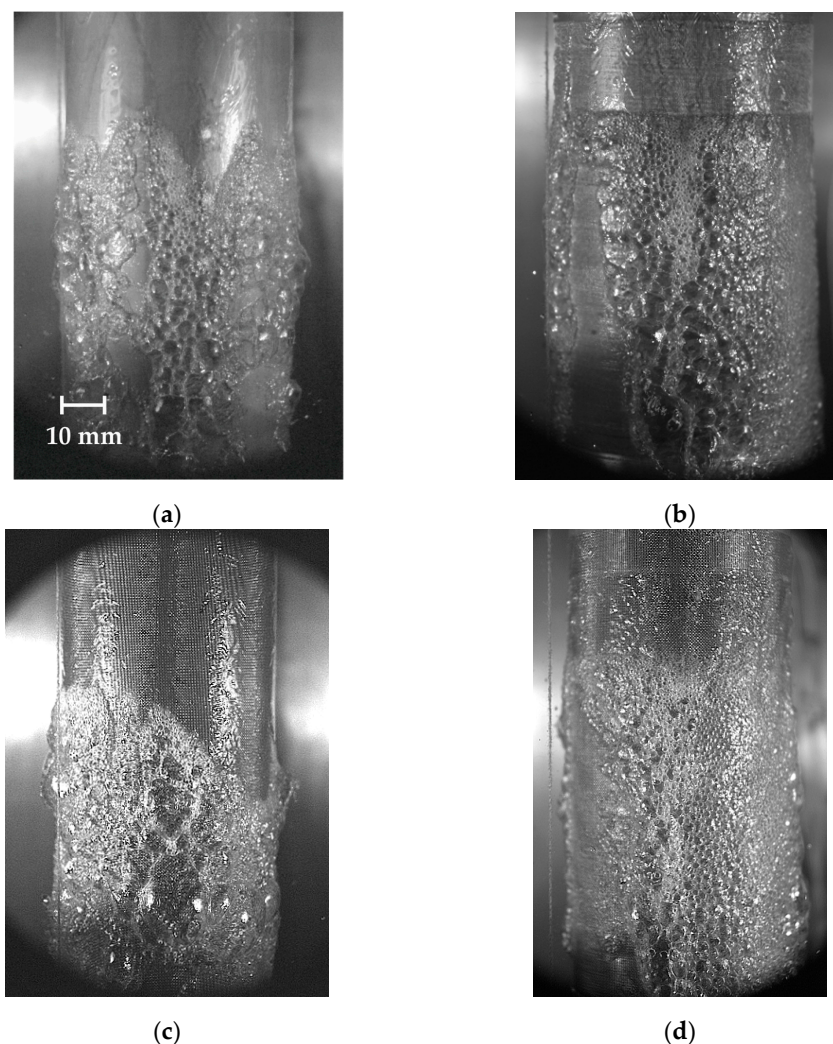
Figure 5. Developed nucleate boiling of R114/R21 mixture on: (**a**) smooth (q = 5.6 W/cm^2, *Re* = 845), (**b**) microstructured by MDC (q = 6.2 W/cm^2, *Re* = 1260), (**c**) covered by mesh (q = 5 W/cm^2, *Re* = 845) and (**d**) combined (q = 5 W/cm^2, *Re* = 1260) surfaces.

(**a**)

(**b**)

(**c**)

(**d**)
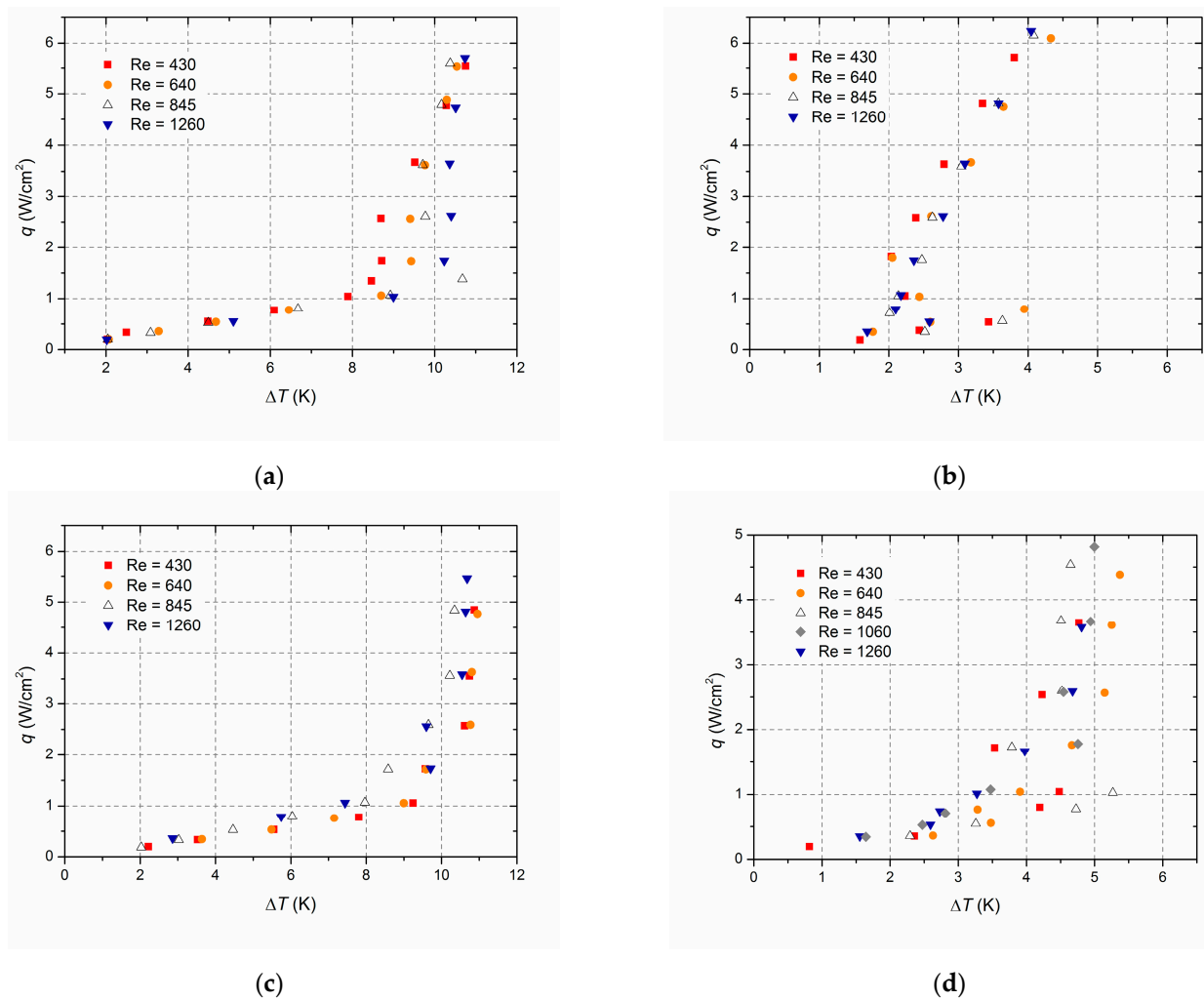
Figure 6. Boiling curves for: smooth (**a**), microstructured by MDC (**b**), smooth covered by mesh (**c**), and combined (**d**) surfaces.

(**a**)

(**b**)
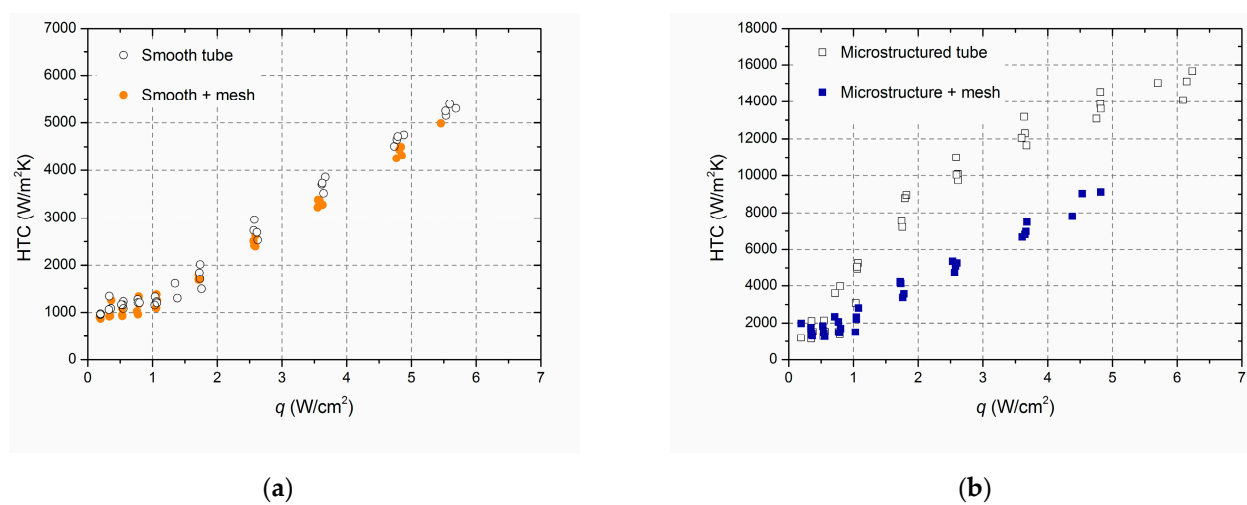
Figure 7. HTC vs. *q* dependencies for: smooth tube and smooth tube, covered by mesh (**a**); microstructured tube and microstructured tube, covered by mesh (**b**).

A brief discussion on the problem of the correct selection of the upper mesh covering parameters is given at the end of the section.

There are not many correlations for predicting pool boiling heat transfer coefficients for microstructured surfaces. We were able to find the calculation dependencies for predicting the pool boiling HTC for microfinned surfaces in [29,30]. Next, we tried to compare the obtained data for the MDC surface with these correlations, assuming that the process of developed nucleate boiling should be very similar for falling films and pool boiling. The main difference is brought by the evaporation of the film, however, in a developed boiling regime, its role decreases to a negligible value. We also neglected the presence of additional longitudinal knurling, present on the MDC-surface over the microfinning, since there are no calculation dependencies for such geometry in the literature (the correlation proposed in [29] for the prediction of boiling on micropin surfaces also gives greatly overestimated values in case of our MDC-surface).

The calculation dependence of Aksyanov et al. [29] has the form:

$$\alpha/\alpha_0 = 6K_q^{-0.2}\left(\frac{\theta}{90}\right)^{0.554}\left(\frac{h}{l_0}\right)^{0.19}\left(\frac{\Delta}{l_0}\right)^{0.201}(\delta/l_0)^{-0.394}, \tag{6}$$

where α, α_0 are the heat transfer coefficients of microstructured and smooth surfaces; K_q is the dimensionless criterion, namely, the scale of the averaged velocity of liquid resulting from a vapor generation process: $K_q = ql_0/(r\rho''\nu')$; l_0 is the Laplace constant $l_0 = \sqrt{\sigma/(g(\rho'-\rho''))}$; ρ' and ρ'' are the liquid and vapor density; ν' is the fluid kinematic viscosity; r is the latent heat of vaporization; σ is the surface tension coefficient. Geometrical parameters are the following: the angle of fin inclination—θ; fin height—h; gap between the fins—Δ; average fin thickness—δ.

The formula for α_0 expresses a standardized heat transfer coefficient:

$$\alpha_0 = 872P_{cr}^{\frac{1}{3}}/\left(T_{cr}^{\frac{5}{6}}M^{\frac{1}{6}}\right)\left(\frac{P}{P_{cr}}\right)^{0.1}\left(1+4.64\left(\frac{P}{P_{cr}}\right)^{1.16}\right)q^{2/3}, \tag{7}$$

where P_{cr} and T_{cr} are the critical pressure and critical temperature of the coolant, and M is the molecular weight of the coolant. The calculation dependence proposed in [29] by Formulas (6) and (7) makes it possible to predict heat transfer without requiring empirical parameters. However, it is worth noting that Formula (7) in our case gave overestimated values of α_0, so we used our own experimental data for smooth surface (Figure 6a) as reference values.

The dependence proposed by Huang [30] has the form of:

$$\alpha = 180\left(\frac{k_l}{l_0\sqrt{2}}\right)\left(\frac{ql_0\sqrt{2}}{k_lT_S}\right)^{0.36}\left(\frac{\rho'}{\rho''}\right)^{0.3}\left(\frac{P_{fin}}{l_0\sqrt{2}}\right)^{-0.2}\left(\frac{\Delta}{l_0\sqrt{2}}\right)^{-0.5}, \tag{8}$$

where k_l is the liquid thermal conductivity; T_S—saturation temperature and P_{fin} is fin pitch.

Comparison of received experimental data on HTC vs. heat flux for microstructured by MDC surface with the correlations for microfinned surfaces (6,8) shown in Figure 8. For reference, Figure 8 also shows the experimental data obtained for a smooth surface. As noted, the heat transfer enhancement on the microstructured tube is about 3–4 times more as compared to the smooth surface even at small heat fluxes, and ONB begins at heat flux values about 2 times less than those for the smooth surface. In fact, the maximal heat transfer enhancement up to 4 times takes place, namely, in the region of small heat fluxes (q: $1 \div 2.6$ W/cm^2) because in this case, we compare the quite developed boiling on the MDC-surface with a highly underdeveloped boiling regime on the smooth surface.

The dependence (6) for a microfinned structure quite well describes the obtained experimental data for the microstructured MDC-surface, even better than within a deviation of 30%, as stated by the authors of [29]. Some excess of the experimental data over the predicted data (here the logarithmic fit of calculated points is implied) in the region of heat fluxes $q \leq 4$ W/cm^2 can be associated with the presence of additional knurling, which

creates partly closed pores and intensifies heat transfer as compared to microfinned surfaces (according to our assumptions), so with the fact that we used the dependence (6) developed for a pool boiling to describe the falling films data: it is known that the contribution of falling film evaporation can give an additional increase in heat transfer as compared to pool boiling, especially at low and moderate heat fluxes, reaching 20–30%. The appearance of a step in the calculated HTC values by (6) in Figure 8 in the region of low heat fluxes $(1 \div 1.8 \text{ W/cm}^2)$ is due to the presence of an underdeveloped boiling regime on the smooth surface with low HTCs, which are substituted into (6) giving low values of α.
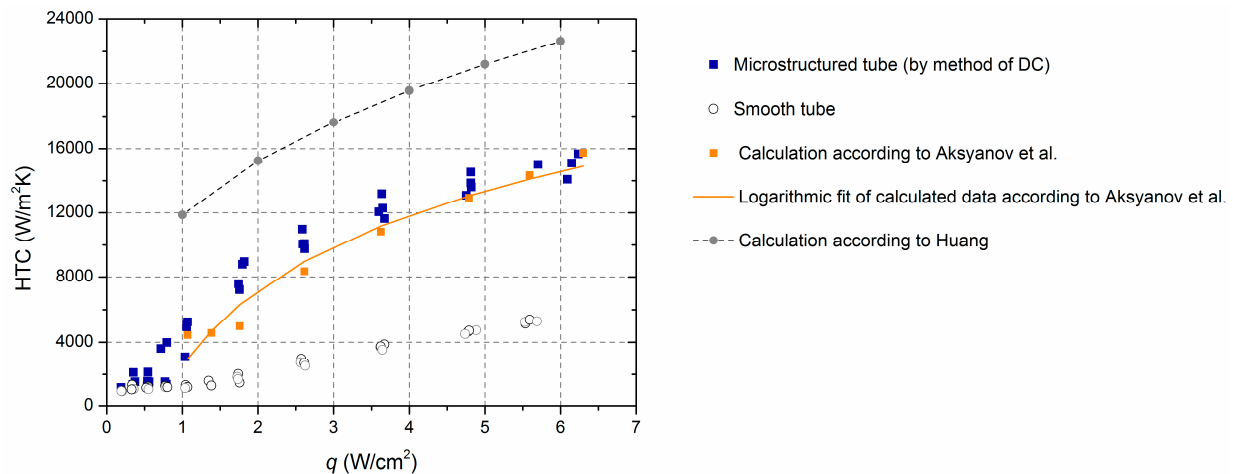
Figure 8. Comparison of HTC vs. q dependence for microstructured by deformational cutting tube with correlations for predicting pool boiling HTC for microfinned surfaces [29,30].

The dependence (8), on the contrary, does not work in our case, about two times exceeding the HTC data obtained, although it can be noted that both correlations have very similar character of the dependence of HTC on the heat flux.

In conclusion, it can be added that next exceeding the heat flux values provided in Figure 8 leads to the flattening of HTC vs. q dependence, associated with the appearance of washable dry spots, beginning from the lower part of the heated tube. Dry spots appear after reaching of CHF in places where the film is thinned, for example, such regions are visible in Figure 5a like bare zones (but in fact, these regions are still covered with a microlayer of liquid film). The microstructured surfaces, similar to those used in this work, in addition to increasing the heat transfer coefficient and reducing the ONB, provide the capillary replenishment of nucleation centers with liquid, making it possible to delay the development of the crisis phenomena. According to our estimates, based on a study of heat transfer on similar MDC-surfaces earlier [22], the minimal increase in CHF on the MDC-surface used in this work may be about 2 times as compared to the smooth surface, namely, to reach about 12 W/cm^2 for the upper values of the passed range of liquid flow rates.

Below, we briefly discuss the possible causes of reducing heat transfer when using the combined coverage.

As already mentioned we attribute the absence of heat transfer enhancement for the stainless steel (AISI 304) mesh-covered smooth copper surface primarily to the low thermal conductivity of the used mesh material ($\lambda \approx 15 \text{ W/mK}$) and the imperfect contact of the mesh with the heated surface (allowing the existence of gaps ~10 microns at the points of contact (despite our attempts to tighten the mesh covering on the tube as closely as possible). Maybe the second reason is even more important because there are works in which it is shown that steel coverings can be effective means of heat transfer. For example, in [31] it is shown that HTC provided by 3D-printed capillary-porous stainless steel coating (LPW 155, $\lambda \approx 20 \text{ W/mK}$) can be higher than HTC of the brass one (AISI C836000, $\lambda \approx 89 \text{ W/mK}$) with the same parameters of porous structure, at boiling of n-dodecane in horizontal liquid layers at reduced pressures. Thus, these issues require additional research.

Also, especially in the case of combined surfaces, we should not discount the possibility that guided by the choice of mesh parameters based on the empirical data of other authors [5,6,8] as well as our own previous data for microstructured surfaces [22], we may not choose the mesh coverage parameters well enough for our experimental conditions, which may cause the deterioration of vapor removal.

Studying the one-layer mesh coverings with an aperture size larger than the bubble departure diameter as well as the order of the departure diameter and smaller than the departure diameter, Tolubinskiy et al. [32] showed that the maximum HTC is realized at an aperture of the order of the bubble departure diameter. Based on this, we can assess that it is also true for the upper layer of two-layer coverings (or combined coatings with mesh covering the basic microstructure, like in our case). Then, the basic microstructure—or fine mesh in the case of two-layer mesh covering—is responsible for the intensification of the nucleation process and the upper coverage at least should not prevent effective vapor removal.

To estimate the value of departure diameter for the R114/R21 refrigerant mixture use the Labuntsov formula [33]:

$$D = 1.8 \left(\frac{\sigma d_0}{g(\rho' - \rho'')} \right)^{1/3} \tag{9}$$

where d_0 is the characteristic size of the microroughness of the heating surface.

Based on Mahmoud and Karayiannis [34] calculation, who used the Hsu model [35] to predict the range of active cavity size for different liquids at atmospheric pressure and 5 K subcooling (5.5–126 μm, 0.7–108 μm, 0.4–79 μm—for water, HFE-7100 and FC-72, respectively), we can assume, without greatly deviating from the truth, that the range of active nucleation sites will be 1–100 μm for the R114/R21 refrigerant mixture (note, that this range includes the transverse dimensions of the gap between microfins, Figure 1b). Substituting the minimum and maximum values of the range into Formula (9) as d_0, we have: $D \approx 190$ μm for the smallest cavities and $D \approx 890$ μm for the biggest ones.

Thus, according to the calculation, by using the mesh covering with an aperture of 220 μm perhaps we are preventing vapor removal. When choosing the mesh parameters, besides basing the choice on our own results on enhancing surfaces microstructure parameters [22], we were guided by the parameters of enhancing covering from [6] (consisting of three upper layers of mesh with aperture 254 μm and diameter 50 μm) as well as by the uniform covering parameters from [8] (with aperture 100 μm and diameter 30 μm)—in both cases, the aperture of upper coverings was significantly less than the bubble departure diameter for water ($D \approx 2$ mm under standard conditions). As a result, our preference was given to mesh with an aperture of 220 μm (available with a wire diameter of 100 μm), slightly exceeding the pitch of the lower microfinning by MDC (200 μm). However, we did not take into account the fact that in previous work [6,8] boiling was carried out at high heat fluxes ~100 W/cm^2, an order of magnitude higher than maximum operating heat fluxes ~10 W/cm^2 in case of boiling refrigerant mixture R114/R21 films. At such high heat fluxes, cavities with the smallest dimensions can be activated. So, the different operating ranges of heat fluxes used in different works may be a possible cause of the discrepancy with respect to the choice of optimal aperture values of upper mesh coverings.

However, these are just some preliminary considerations, the issue of choosing covering geometrical parameters requires more precise analysis and calculations.

4. Conclusions

The experimental data on heat transfer coefficients at evaporation and boiling of a refrigerant mixture R114/R21 film falling over the smooth or microstructured surfaces and the same surfaces, covered by micromesh, are obtained. It is shown that:

- A microstructured surface created by deformational cutting demonstrates significant heat transfer enhancement—up to four times as compared to the smooth surface.

- Adding mesh covering with an aperture of 220 µm reduces the enhancement reached on the microstructured surface alone by up to two times. Thus, the heat transfer enhancement, provided by a combined surface, is about two times as compared to the smooth surface.
- The chosen mesh coverage overlaying the smooth surface does not give heat transfer enhancement compared to the smooth surface.
- The absence or deterioration of heat transfer enhancement on studied mesh-covered surfaces can be associated with the low thermal conductivity of used mesh material and especially the imperfectness of the mesh mounting method. The applied mesh covering possibly prevents the effective vapor removal during the boiling of the R114/R21 mixture falling film.
- The correlation, proposed by Aksyanov et al. for predicting the pool boiling heat transfer on microfinned surfaces, describes the obtained film flow data on heat transfer on the MDC surface quite well, while the correlation of Huang gives twice the values of the heat transfer coefficient.

Nomenclature

A	heat releasing surface area
C	correction factor
D	bubble departure diameter
d	tube diameter; characteristic size of microroughness
G	mass flow rate
g	gravity acceleration
h	heat transfer coefficient; fin height
I	current through the heating element
k_l	liquid thermal conductivity
l_0	Laplace constant
P	Pressure
P_{fin}	fin pitch
q	heat flux density
R	heating element resistance
R_a	mean roughness
Re	film Reynolds number, $Re = \frac{4G}{\pi d \mu}$
T	temperature
U	uncertainty
Greek symbols	
α	heat transfer coefficient
Δ	gap between the fins
δ	liquid film thickness, average fin thickness
δ_{gap}	size of gap between fin tips

θ	the angle of fin inclination
λ	thermal conductivity
μ	dynamic viscosity
ρ	Density
σ	surface tension
Subscripts	
cr	Critical
s	Saturation
w	Wall
Superscripts	
′	liquid phase
″	vapor phase

References

1. Huang, Y.; Wang, M.; Xu, L.; Deng, J. Experimental study on a spray and falling-film cooling system. *Case Stud. Therm. Eng.* **2021**, *26*, 101057. [CrossRef]
2. Liang, G.; Mudawar, I. Review of pool boiling enhancement by surface modification. *Int. J. Heat Mass Transf.* **2019**, *128*, 892–933.
3. Dedov, A.V. A Review of Modern Methods for Enhancing Nucleate Boiling Heat Transfer. *Therm. Eng.* **2019**, *66*, 881–915. [CrossRef]
4. Volodin, O.A.; Pecherkin, N.I.; Pavlenko, A.N. Heat Transfer Enhancement at Boiling and Evaporation of Liquids on Modified Surfaces—A Review. *High Temp.* **2021**, *59*, 405–432. [CrossRef]
5. Volodin, O.A.; Pavlenko, A.N.; Pecherkin, N.I. Heat Transfer Enhancement on Multilayer Wire Mesh Coatings and Wire Mesh Coatings Combined with Other Surface Modifications—A Review. *J. Eng. Thermophys.* **2021**, *30*, 563–596. [CrossRef]
6. Zhang, S.; Jiang, X.; Li, Y.; Chen, G.; Sun, Y.; Tang, Y.; Pan, C. Extraordinary Boiling Enhancement Through Micro-Chimney Effects in Gradient Porous Micromeshes for High-Power Applications. *Energy Convers. Manag.* **2020**, *209*, 112665. [CrossRef]
7. Asakavičius, J.P.; Zukauskas, A.A.; Gaigalis, V.A.; Eva, V.K. Heat Transfer from Freon-113, Ethyl Alcohol and Water with Screen Wicks. *Heat Transf. Sov. Res.* **1979**, *11*, 92–100.
8. Tang, K.; Bai, J.; Chen, S.; Zhang, S.; Li, J.; Sun, Y.; Chen, G. Pool Boiling Performance of Multilayer Micromeshes for Commercial High-Power Cooling. *Micromachines* **2021**, *12*, 980. [CrossRef]
9. Sloan, A.; Penley, S.; Wirtz, R.A. Sub-Atmospheric Pressure Pool Boiling of Water on a Screen-Laminate Enhanced Surface. In Proceedings of the 25th Annual IEEE Semiconductor Thermal Measurement and Management Symposium, San Jose, CA, USA, 15–19 March 2009.
10. Tsay, J.Y.; Yan, Y.Y.; Lin, T.F. Enhancement of Pool Boiling Heat Transfer in a Horizontal Water Layer Through Surface Roughness and Screen Coverage. *Heat Mass Transf.* **1996**, *32*, 17–26. [CrossRef]
11. Brautsch, A.; Kew, P.A. The Effect of Surface Conditions on Boiling Heat Transfer from Mesh Wicks. In *International Heat Transfer Conference Digital Library*; Begel House Inc.: Danbury, CT, USA, 2002.
12. Chien, L.H.; Tsai, Y.L. An Experimental Study of Pool Boiling and Falling Film Vaporization on Horizontal Tubes in R-245fa. *Appl. Therm. Eng.* **2011**, *31*, 4044–4054. [CrossRef]
13. Chien, L.H.; Hwang, H.L. An Experimental Study of Boiling Heat Transfer Enhancement of Mesh-on-Fin Tubes. *J. Enhanc. Heat Transf.* **2012**, *19*, 75–86. [CrossRef]
14. Kim, H.; Park, Y.; Kim, H.; Lee, C.; Jerng, D.W.; Kim, D.E. Critical Heat Flux Enhancement by Single-Layered Metal Wire Mesh with Micro and Nano-Sized Pore Structures. *Int. J. Heat Mass Transf.* **2017**, *115*, 439–449. [CrossRef]
15. Dąbek, L.; Kapjor, A.; Orman, Ł.J. Distilled Water and Ethyl Alcohol Boiling Heat Transfer on Selected Meshed Surfaces. *Mech. Ind.* **2019**, *20*, 701. [CrossRef]
16. Zhang, C.; Zhang, L.; Xu, H.; Li, P.; Qian, B. Performance of Pool Boiling with 3D Grid Structure Manufactured by Selective Laser Melting Technique. *Int. J. Heat Mass Transf.* **2019**, *128*, 570–580. [CrossRef]
17. Pastuszko, R.; Kaniowski, R.; Wójcik, T.M. Comparison of Pool Boiling Performance for Plain Micro-Fins and Micro-Fins With a Porous Layer. *Appl. Therm. Eng.* **2020**, *166*, 114658. [CrossRef]
18. Huang, S.; Wang, L.; Pan, Z.; Zhou, Z. Experimental Investigation of a New Hybrid Structured Surface for Subcooled Flow Boiling Heat Transfer Enhancement. *Appl. Therm. Eng.* **2021**, *192*, 116929. [CrossRef]
19. Chen, G.; Fan, D.; Zhang, S.; Sun, Y.; Zhong, G.; Wang, Z.; Wan, Z.; Tang, Y. Wicking capability evaluation of multilayer composite micromesh wicks for ultrathin two-phase heat transfer devices. *Renew. Energy* **2021**, *163*, 921–929. [CrossRef]
20. Hu, Y.; Lei, Y.; Liu, X.; Yang, R. Heat transfer enhancement of spray cooling by copper micromesh surface. *Mater. Today Phys.* **2022**, *28*, 100857. [CrossRef]
21. Smakulski, P.; Sławomir, P. A review of the capabilities of high heat flux removal by porous materials, microchannels and spray cooling techniques. *Appl. Therm. Eng.* **2016**, *104*, 636–646. [CrossRef]
22. Volodin, O.; Pecherkin, N.; Pavlenko, A.; Zubkov, N. Surface Microstructures for Boiling and Evaporation Enhancement in Falling Films of Low-Viscosity Fluids. *Int. J. Heat Mass Transf.* **2020**, *55*, 119722. [CrossRef]

23. Zubkov, N.N.; Ovchinnikov, A.I.; Vasil'ev, S.G. Tool–workpiece interaction in deformational cutting. *Russ. Eng. Res.* **2016**, *36*, 209–212. [CrossRef]

24. Zubkov, N.; Poptsov, V.; Vasiliev, S. Surface Hardening by Turning without Chip Formation. *Jordan J. Mech. Ind. Eng.* **2017**, *11*, 13–19.

25. Pecherkin, N.I.; Pavlenko, A.N.; Volodin, O.A. Heat transfer and critical heat flux at evaporation and boiling in refrigerant mixture films falling down the tube with structured surfaces. *Int. J. Heat Mass Transf.* **2015**, *90*, 149–158. [CrossRef]

26. Zhukov, V.E.; Mezentseva, N.N.; Pavlenko, A.N. Teplootdacha Pri Kipenii Na Modifitsirovannoy Poverhnosti Vo Freone R21 I Smesi Freonov R114/R21 (Boiling Heat Transfer on Modified Surface in R21 Freon and in R114/R21 Freon Mixture). In Proceedings of the XXXVIII Siberian Thermophysics Seminar dedicated to the 65th Anniversary of the Kutateladze Institute of Thermophysics SB RAS, Novosibirsk, Russia, 29–31 August 2022; pp. 106–111. (In Russian).

27. Dang, C.; Jia, L.; Peng, Q.; Huang, Q.; Zhang, X. Experimental and analytical study on nucleate pool boiling heat transfer of R134a/R245fa zeotropic mixtures. *Int. J. Heat Mass Transf.* **2018**, *119*, 508–522. [CrossRef]

28. Shamirzaev, A. On the Pressure Drop Calculation During the Flow of Two-Phase Non-Azeotropic Mixtures. *Int. J. Multiph. Flow* **2022**, 104314. [CrossRef]

29. Aksyanov, R.A.; Kokhanova, Y.S.; Kuimov, E.S.; Gortyshov, Y.F.; Popov, I.A. Recommendations for Improving the Efficiency of Radio-Electronic Equipment Cooling Systems. *Russ. Aeronaut.* **2021**, *64*, 291–296. [CrossRef]

30. Huang, L.D. Pool Boiling Correlations for Structured Fin Tubes. In Proceedings of the 10th International Conference on Boiling and Condensation Heat Transfer, Nagasaki, Japan, 12–15 March 2018.

31. Shvetsov, D.A.; Pavlenko, A.N.; Brester, A.E.; Zhukov, V.I. Inversiya Crivoy Kipeniya Na Mikrostrukturirovannyh Poristyh Pokrytiyah (Boiling Curve Inversion on Microstructured Porous Coatings). In Proceedings of the 8th Russian national conference on heat transfer "PHKT-8", Moscow, Russia, 17–22 October 2022; pp. 83–84. (In Russian).

32. Tolubinskiy, V.I.; Antonenko, V.A.; Ivanenko, G.V. Crisis Phenomena in Boiling on Submerged Wire Mesh-Wrapped Wall. *Heat Transf. Sov. Res.* **1989**, *21*, 531–535.

33. Labuntsov, D.A. Heat Transfer and Vapor Dynamics. In *Current Concepts of the Mechanism of Nucleate Boiling of Liquids*; Institute of High Temperatures: Moscow, Russia, 1974; Available online: https://inis.iaea.org/collection/NCLCollectionStore/_Public/06/171/6171615.pdf (accessed on 28 November 2022).

34. Mahmoud, M.M.; Karayiannis, T.G. Pool boiling review: Part I–Fundamentals of boiling and relation to surface design. *Therm. Sci. Eng. Prog.* **2021**, *25*, 101024. [CrossRef]

35. Hsu, Y.Y. On the size range of active nucleation cavities on a heating surface. *J. Heat Transf.* **1962**, *84*, 207–213. [CrossRef]